Heavy-ion collision basics

D. Miśkowiec

GSI Helmholtzzentrum für Schwerionenforschung GmbH, Darmstadt, Germany

Basic concepts and terminology of relativistic heavy-ion collision physics are introduced and illustrated by experiment results. Most plots are taken from a recent ALICE overview paper [1].

1 Stages of a heavy-ion collision

The main stages of a Pb–Pb collision at the LHC are shown in Fig. 1. The initial state depends on the collision centrality, the distribution of nucleons within the colliding nuclei, and the nuclear parton distribution functions. The Lorentz-contracted colliding nuclei pass through each other and the space between their receding disks is filled with energy in form of gluons and quarks (quark-gluon plasma). It is convenient to consider collisions between pairs of nucleons [2]. The temporal sequence of these collisions does not depend on their longitudinal positions within nuclei. Instead, all nucleon–nucleon (NN) collisions are initiated at the same time and their duration depends on their hardness. Hard collisions finish first and get all the energy they want; this is why they scale with the number of NN collisions N_{coll}. Soft collisions take longer and compete among themselves for energy, so soft particles scale with the total available energy
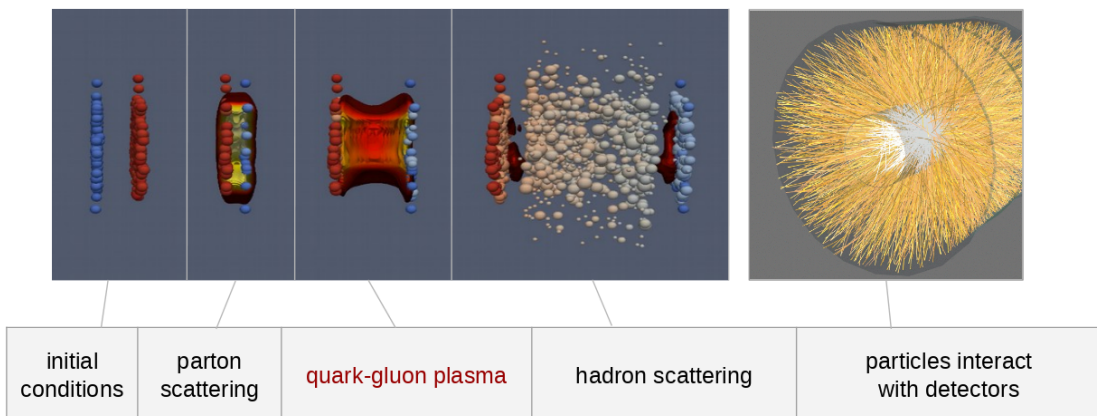

Figure 1 – Main stages of a Pb–Pb collision at the LHC. Sketch taken from Ref.[3]. See text for explanation.

or the number of participating nucleons, N_{part}. Hard collisions do not compete against soft collisions because they are faster, and do not compete among themselves because they are rare. Heavy quarks and high-p_{T} quarks and gluons originate from the initial hard processes. During subsequent reaction stages they interact with the bulk matter probing its properties. The fireball keeps expanding until the energy density drops below 1 GeV/fm^3, at which point the quarks and gluons have to turn into color-neutral hadrons. These still interact with each other for some time, then propagate freely to the detectors.

2   Initial conditions

The initial state depends on the collision centrality, the transverse distribution of nucleons within the colliding nuclei, and the nuclear parton distribution functions. Knowing the nuclear collision cross section $\mathrm{d}\sigma/\mathrm{d}b = 2\pi b$ (for b smaller than the sum of the radii of the two nuclei) and assuming that the multiplicity of the produced particles decreases with increasing b, the centrality can be estimated from the particle multiplicity or any observable proportional to it. Its differential cross section has to be integrated from the right and normalized to the known total collision cross section. As an example, events with centrality 0–5% in ALICE are selected by requiring a particular detector (V0M) signal to be above $26 \cdot 10^3$ (Fig. 2 left). This centrality corresponds [4] to $0 < b < 3.5$ fm. For a fixed b, the fireball shape will still depend on the transverse distribution of energy as resulting from the nucleon positions prior to the collision (Fig. 2 right). The third
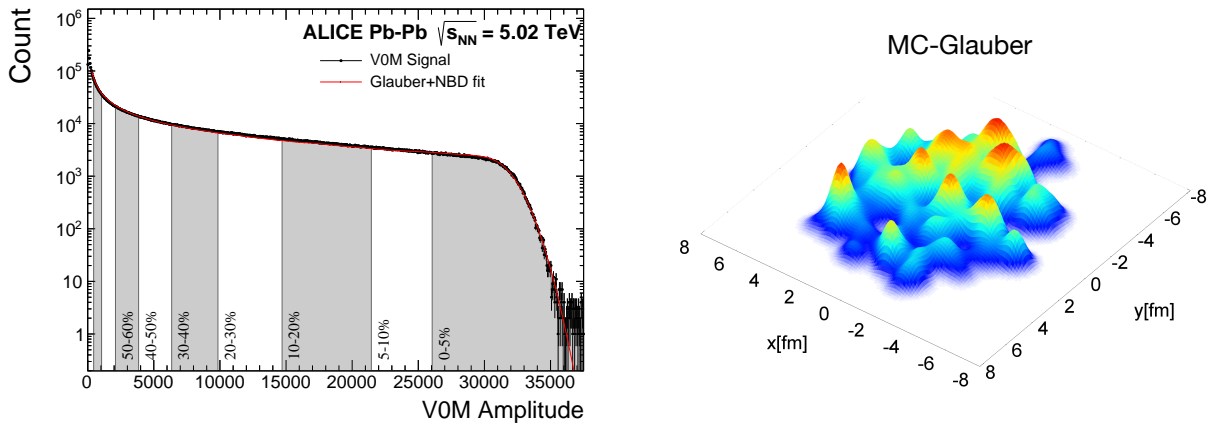

Figure 2 – Initial conditions of a relativistic nucleus–nucleus collision: nucleus–nucleus centrality (left) and the transverse distribution of energy as resulting from nucleon positions in the nuclei (right). Plots from Ref. [1].

ingredient of the initial conditions are the parton distribution functions in nucleons, which differ from those of free protons (shadowing). They can be studied, in the relevant Bjorken-x range, e.g. by measuring W production in proton–nucleus collisions (Fig. 3).
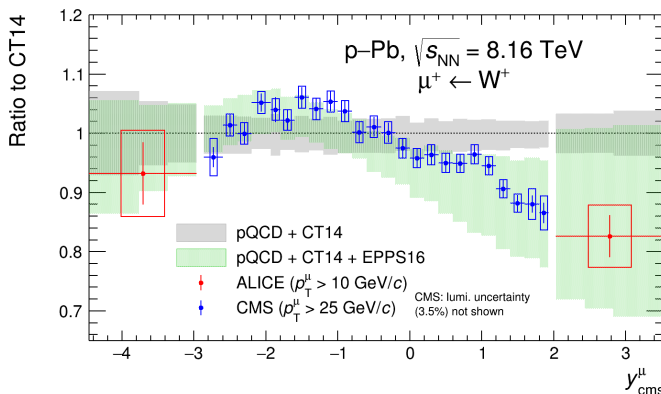

Figure 3 – CMS and ALICE data on W-boson production in p–Pb collisions at the LHC [1]. This measurement is sensitive to the parton distribution function in Pb nucleons.

3 Parton scattering

Heavy quarks are produced in qq̄ pairs in the initial parton scatterings with high momentum transfer. Their final fate – the hadrons in which they end up and the momenta thereof – depend on the subsequent stages of the system evolution, in particular on their interaction with the quark-gluon plasma and, apparently, on the environment in which they hadronize (Fig. 4).
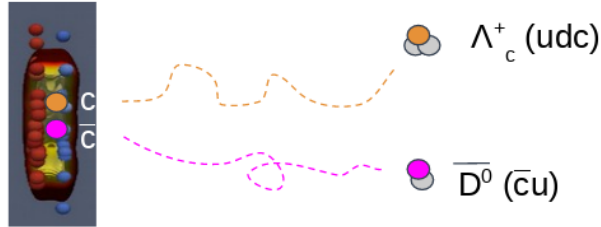

Figure 4 – Charm quarks are produced in the initial parton scattering, interact with the expanding QGP, and hadronize into charmed mesons and baryons.

A standard way of quantifying the interaction of heavy quarks with the QGP consists in comparing the transverse momentum spectra of hadrons carrying these quarks in nucleus–nucleus (AA) and pp collisions. The nuclear modification factor is defined as

$$R_{\text{AA}}(p_{\text{T}}) = \frac{1}{\langle N_{\text{coll}} \rangle} \frac{\text{d}N_{\text{AA}}/\text{d}p_{\text{T}}}{\text{d}N_{\text{pp}}/\text{d}p_{\text{T}}} \tag{1}$$

with $\langle N_{\text{coll}} \rangle$ being the number of nucleon–nucleon collisions within the nucleus–nucleus collision, averaged over the centrality bin. Since hard processes scale with the number of nucleon–nucleon collisions, R_{AA} would be unity for (hypothetical) non-interacting heavy quarks (except for shadowing), as it is indeed the case for hard direct photons and W bosons.

4 Quark-gluon plasma

Before one can study the interaction of heavy quarks with the QGP, the geometry and expansion of the QGP itself must be known. The collective longitudinal and transverse expansion (aka flow) of the QGP are here the main features. "Collectivity" can be defined as the lack of independence between the positions and velocities of the particles/fluid elements. The longitudinal expansion results mainly from the dependence of particle position (at a finite time) on the particle velocity (at the time of the full overlap of the two colliding nuclei). The transverse expansion, on the other hand, is driven by the preferred direction of emission of particles away from the opaque high-density zone. In non-central collisions, the transverse expansion may depend on the azimuthal angle. These modes of flow, sketched in Fig. 5, influence the momenta of emitted particles.
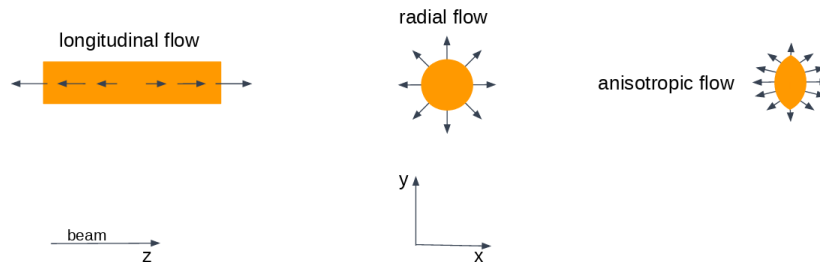

Figure 5 – Longitudinal and transverse flow in relativistic heavy-ion collisions.

The elliptic flow, quantified by the second Fourier harmonic of the azimuthal distribution of particles with respect to the reaction plane, is a particularly interesting observable. The reaction

plane is defined by the beam axis and the impact parameter. The collision energy dependence of the elliptic flow parameter v_2 in midcentral (20–30%) lead and gold collisions is shown in Fig. 6. The preferred emission of particles at the lowest and highest energy is in plane, while at 1.5–3 GeV the in-plane emission is obstructed by the presence of the non-overlapping parts of the colliding nuclei (spectators).
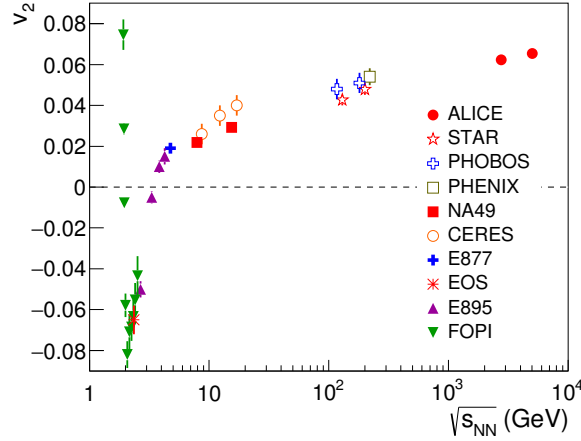

Figure 6 – Collision energy dependence of the elliptic flow in midcentral (20–30%) lead and gold collisions [1].

The high values of v_2 observed at 130–200 GeV at RHIC were in agreement with hydrodynamic calculations, indicating that the QGP behaved like a non-viscous liquid rather than a gas of non-interacting quarks and gluons as had been initially expected. Viscosity would smear out the velocity fields and thus would reduce v_2, this was not observed. A big question was whether v_2 would be lower at the LHC. It turned out that the QGP there was as liquid and as perfect as at RHIC; the v_2 is even slightly higher, but this is only because of its scaling with p_T.

Heavy quarks and high-momentum particles are important probes of the QGP. Energetic (faster than bulk) heavy quarks have to traverse the QGP before they can leave the fireball. The energy loss they experience, combined with the steeply falling hadron p_T spectra, leads to a reduced value of R_{AA} (Fig. 7 left). Slight differences between the particle species (mass ordering) reflect the radiative energy loss differences related to the dead cone effect [5]. The interaction of heavy quarks with the QGP and the fact that the final charm and beauty hadrons contain also light quarks lead to these hadrons showing an azimuthal anisotropy of emission similar to light hadrons, albeit reduced in strength (Fig. 7 right).
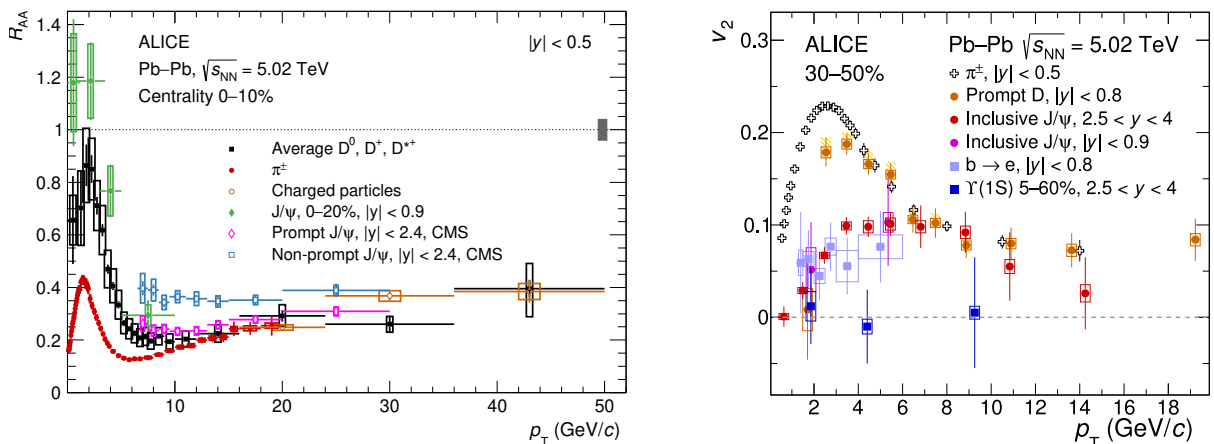

Figure 7 – Nuclear modification factor R_{AA} (left) and elliptic flow parameter v_2 (right) of various particle species. Non-prompt J/ψ mesons come from beauty decays and thus are a proxy for b quarks. The left and right plots are taken from Refs. [6] and [1], respectively.

The suppression of charmonia and bottomonia, and especially of their higher states, is another important signature of the presence of the QGP. Quarkonia, if at all formed, can dissociate into c and c̄ (or b and b̄) by the interaction with the QGP before they have a chance of leaving the fireball (Fig. 8 left). The suppression of bottomonium in Pb–Pb collisions at the LHC is clearly seen in the CMS data shown in the right panel of Fig. 8.
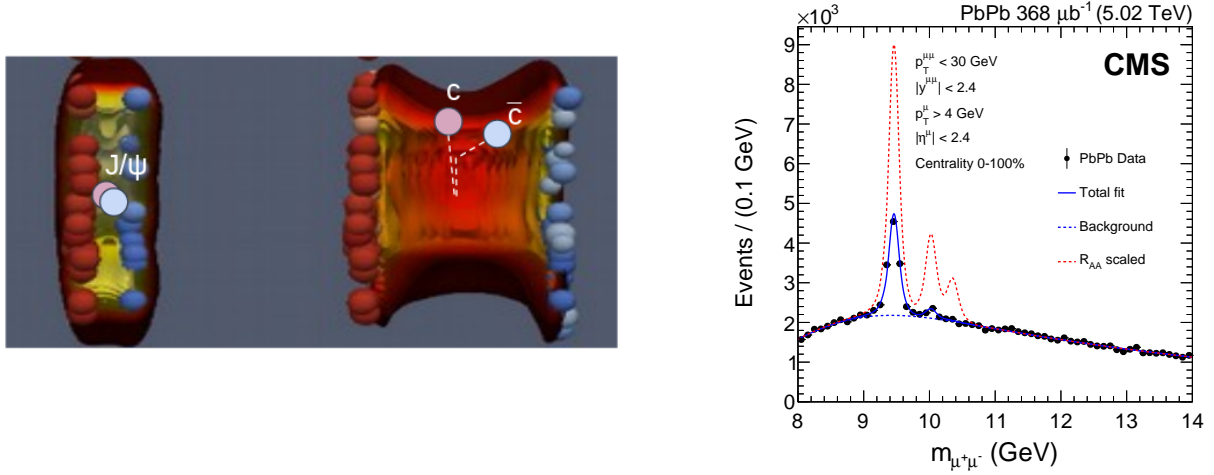

Figure 8 – Left: J/ψ creation in the initial parton scattering and possible dissociation in the QGP. Right: Suppression of $\Upsilon(1S)$, $\Upsilon(2S)$, and $\Upsilon(3S)$ in Pb–Pb collisions compared to pp (figure taken from Ref. [7]).

5 Hadronization

The critical temperature at which the QGP turns back into hadrons is 155 MeV [8,9]. At the LHC the standard vacuum fragmentation process known from e^+e^- colliders seems to be augmented by another hadronization mechanism, quark coalescence. Indications for this can be found in the J/ψ yield and in the charm fragmentation fractions. With about 15 $c\bar{c}$ pairs produced per unit rapidity, the predicted [11] additional production of J/ψ via c–c̄ (re)combination (or J/ψ (re)generation) seems indeed to enhance the low-p_T J/ψ yield in the most central Pb–Pb collisions (Fig. 9 left). Another hint for quark coalescence can be found in the charm fragmentation fractions. The relative abundance of Λ_c in pp is significantly enhanced – and D^0 reduced – compared to the ee and ep collision experiments (Fig. 9 right).
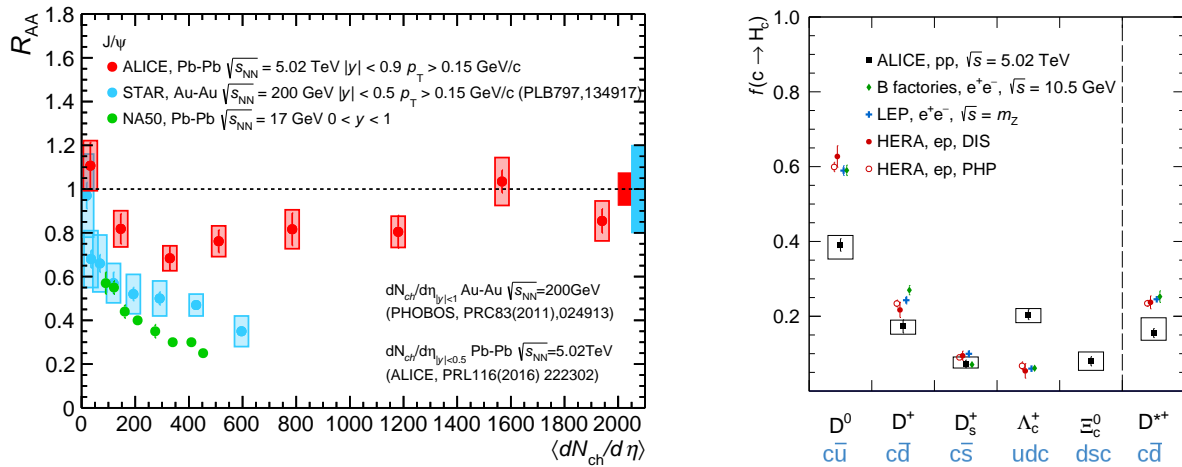

Figure 9 – Left: Nuclear modification factor of J/ψ [1]. In the most central Pb–Pb collisions, the suppression is compensated by an additional production channel of J/ψ via c–c̄ (re)combination. Right: fragmentation fractions of c quarks in pp collisions [10]. The baryon/meson ratio is enhanced in pp compared to ee and ep collisions.

6 Hadron scattering

The freshly formed hadrons may scatter before the density drops enough to allow for their free propagation to detectors. The yields of hadron species get fixed when the inelastic interactions cease (chemical freezeout). Similarly, the end of elastic interactions (kinetic freezeout) shapes the transverse momentum spectra of hadrons. The chemical freezeout temperature, extracted from the hadron yields (Fig. 10) is about 156 MeV, thus coinciding with the critical temperature at which the hadronization takes place.
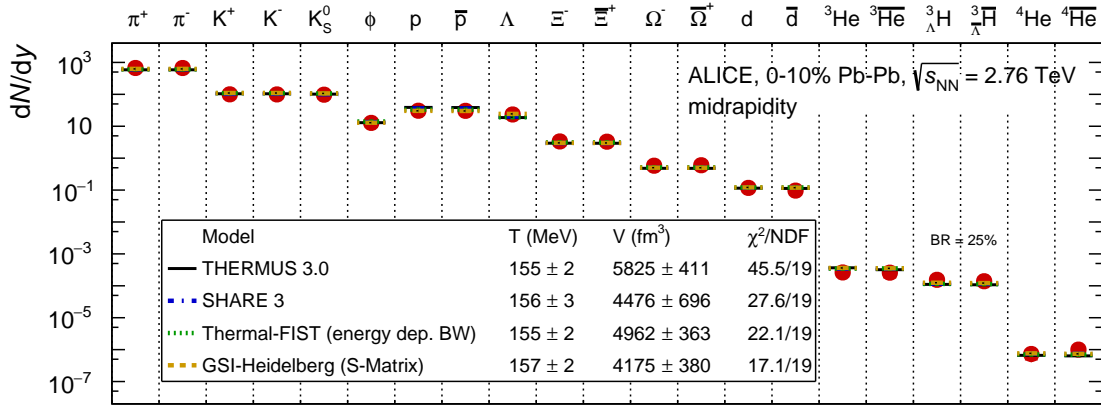

Figure 10 – Hadron yields and their description by the statistical model [1]. The extracted chemical freezeout temperature is 155–157 MeV, similar to the critical temperature at which the QGP turns into hadrons.

The kinetic freezeout is explored by simultaneously fitting the shapes of the transverse momentum spectra of various hadrons with just two parameters representing the temperature and the transverse flow velocity. This so-called "blast-wave fit" yields temperatures between 100 and 160 MeV depending on the treatment of resonances which feed into light mesons, and thus leaving – or not – room for the hadronic scattering stage in the evolution of the fireball [1]. The presence of a hadronic stage is supported e.g. by the observed reduction of K* ($c\tau = 4.2$ fm) yield in central Pb–Pb collisions, presumably caused by scattering of its decay daughter pion.

7 Conclusions

While the main object of study in relativistic heavy-ion collisions is the quark-gluon plasma, a detailed understanding of all stages of the reaction is necessary for proper interpretation of the measurements. The author thanks for the invitation to Moriond and acknowledges the pleasant and inspiring atmosphere of the meeting.

References

1. ALICE Collaboration, arXiv:2211.04384 [nucl-ex].
2. A Białas, M Bleszyński, and W Czyż, Nucl. Phys. B 111(1976)461.
3. H. Petersen and J. Bernhard, MADAI collaboration.
4. http://www.gsi.de/~misko/overlap/interface.html
5. Y. L. Dokshitzer and D. E. Kharzeev, Phys. Lett. B519 (2001) 199, arXiv:hep-ph/0106202.
6. ALICE Collaboration, JHEP 01 (2022) 174, arXiv:2110.09420.
7. CMS Collaboration, Phys. Lett. B 790 (2019) 270, arXiv:1805.09215 [hep-ex].
8. A. Bazavov et al., Phys. Rev. D 90 (2014) 094503, arXiv:1407.6387 [hep-lat].
9. S. Borsanyi et al., Phys. Lett. B 730 (2014) 99–104, arXiv:1309.5258 [hep-lat].
10. ALICE Collaboration, Phys. Rev. D 105, L011103 (2022), arXiv:2105.06335 [nucl-ex].
11. P. Braun-Munzinger and J. Stachel, Phys. Lett. B490 (2000) 196, arXiv:nucl-th/0007059.